Iron control on global productivity: an efficient inverse model of the ocean's coupled phosphate, silicon, and iron cycles

Benoit Pasquier and Mark Holzer

School of Mathematics and Statistics, UNSW
b.pasquier@student.unsw.edu.au, mholzer@unsw.edu.au

1. Introduction

The global ocean ecosystem is controlled by biological production, which is governed by the physical constraints of temperature, light and nutrient availability on oceanic phytoplankton. It is common to assume a single macronutrient as globally limiting, which makes it possible to build simple models that capture the major nutrient cycles surprisingly well. However, it has been shown that complex co-limitation processes are at play in global biogeochemical cycles. For example, the existence of HNLC regions is attributed to iron limitation [e.g., *Boyd et al.*, 2007; *Landry et al.*, 1997]. To understand how the global ocean ecosystem responds to climate-driven changes in the iron supply, it is therefore crucial to have a model that couples the major nutrient cycles to the iron cycle. This allows us to investigate how the global-scale teleconnections of the marine ecosystem respond to changes in micronutrients under various scenarios. Our work here is motivated by the following questions:

1. Can we constrain the biogeochemical parameters of the coupled phosphorus, silicon and iron cycles?
2. How do the coupled nutrient cycles respond to perturbations in the aeolian iron supply?
3. How are phosphate and opal export production affected?
4. What is the response of the biomass fraction of diatoms?
5. What are the transient timescales for abrupt perturbations?

We begin by describing a simple inverse model that we have dubbed FePSi. FePSi couples dissolved iron to the marine phosphorous and silicon cycles.

2. The FePSi model

The tracer equations for the nutrient concentrations are given by:

$$\partial_t \begin{bmatrix} p \\ f \\ s \end{bmatrix} + \begin{bmatrix} \mathcal{T} & & \\ & \mathcal{T} & \\ & & \mathcal{T} \end{bmatrix} \begin{bmatrix} p \\ f \\ s \end{bmatrix} = B + S$$

- p is the **phosphate** concentration [PO_4].
- f is the **dissolved iron** concentration [Fe_T].
- s is the **silicic acid** concentration [$Si(OH)_4$].
- $\mathcal{T}$ is the **advective-eddy-diffusive transport operator** from the global steady state data-assimilated circulation of *Primeau et al.* [2013].
- B is the **biogenic transport** of all three tracers (detailed below).
- S is the sum of **external sources and sinks of iron** (aeolian dust deposition, hydrothermal vents, sediments, and organic scavenging) modeled as in the work of *Frants et al.* [2016].

We consider 3 functional classes of phytoplankton: Diatoms, Large and Small. The biogenic transport is:

$$B = \sum_e \begin{bmatrix} \mathcal{S}_c^P U_c \\ \mathcal{S}_c^{Fe} R_{f:p}(f) U_c \\ \mathcal{S}_c^{Si} R_{s:p}(s) U_c \end{bmatrix} - \sum_e \begin{bmatrix} U_c \\ R_{f:p}(f) U_c \\ R_{s:p}(s) U_c \end{bmatrix}$$

- c is the phytoplankton class (= D, L or S).
- The $\mathcal{S}$'s are **sinking and remineralization operators** redistributing a fraction $1-\sigma_c$ that is taken up by a given class throughout the water column (with power-law Martin profiles) as instantly remineralized phosphate, iron, or silicic acid.
- $R_{f:p}$ is the **(Fe:P) uptake ratio** as in *Galbraith et al.* [2010]:

$$R_{f:p} = R_0 \frac{f}{f + k_{Fe:P}}$$

- $R_{s:p}$ is the **(Si:P) uptake ratio** as in *Matsumoto et al.* [2013]:

$$R_{s:p} = R_{min} + \frac{s}{s + k_{Si:P}}(R_{max} - R_{min})$$

- U_c is the **phosphate uptake rate**. It is equal to "growth rate" × "population density":

$$U_c = \mu_c P_c$$

For each class c, its population density P_c satisfies a logistic equation and is assumed to have reached its steady state quickly on the timescales of the circulation:

$$\partial_t P_c = \mu_c P_c - \lambda_c \left(\frac{P_c}{P_c^*}\right) P_c \implies P_c = \left(\frac{\mu_c}{\lambda_c}\right) P_c^*$$

Here μ_c is the growth rate, λ_c is the mortality rate, and both are defined by:

$$\begin{cases} \mu = \mu_0 F_T F_I F_N \\ \lambda = \lambda_0 F_T \end{cases}$$

- μ_0, λ_0 are the **optimal growth and mortality rates** at 0°C.
- F_T is the **temperature limitation** [*Eppley*, 1972].
- F_I is the **light limitation** as in *Galbraith et al.* [2010].
- F_N is the **nutrient limitation**.

The nutrient limitation is constructed in terms of Michaelis-Menten factors for each nutrient (with class-specified half-saturation rates):

$$F_N = \min\left(\frac{p}{p+k_p}, \frac{f}{f+k_f}, \frac{s}{s+k_s}\right)$$

PARAMETER OPTIMISATION

Tracer concentrations are discretized onto a 3D grid and organized into column vectors, so that all linear operators become matrices. Note, however, that the equations are nonlinear. We efficiently solve for the steady state using an iterative Newton root search method. The efficient numerics allow us to optimize the following parameters by minimizing the mismatch with observed nutrient concentrations, dissolved iron, and chlorophyll:

- P_D^*, P_L^*, and P_S^* which set the Diatom, Large and Small phytoplankton population sizes.
- R_0 the scale of the (Fe:P) uptake ratio.
- R_{max} and R_{min} which set the (Si:P) uptake ratio.
- σ_D, σ_L, and σ_S (in the sinking+remineralization operator $\mathcal{S}$), which set the fraction of uptake recycled locally.

3. Climatological base state

Phosphate and silicic acid, mismatch with observations
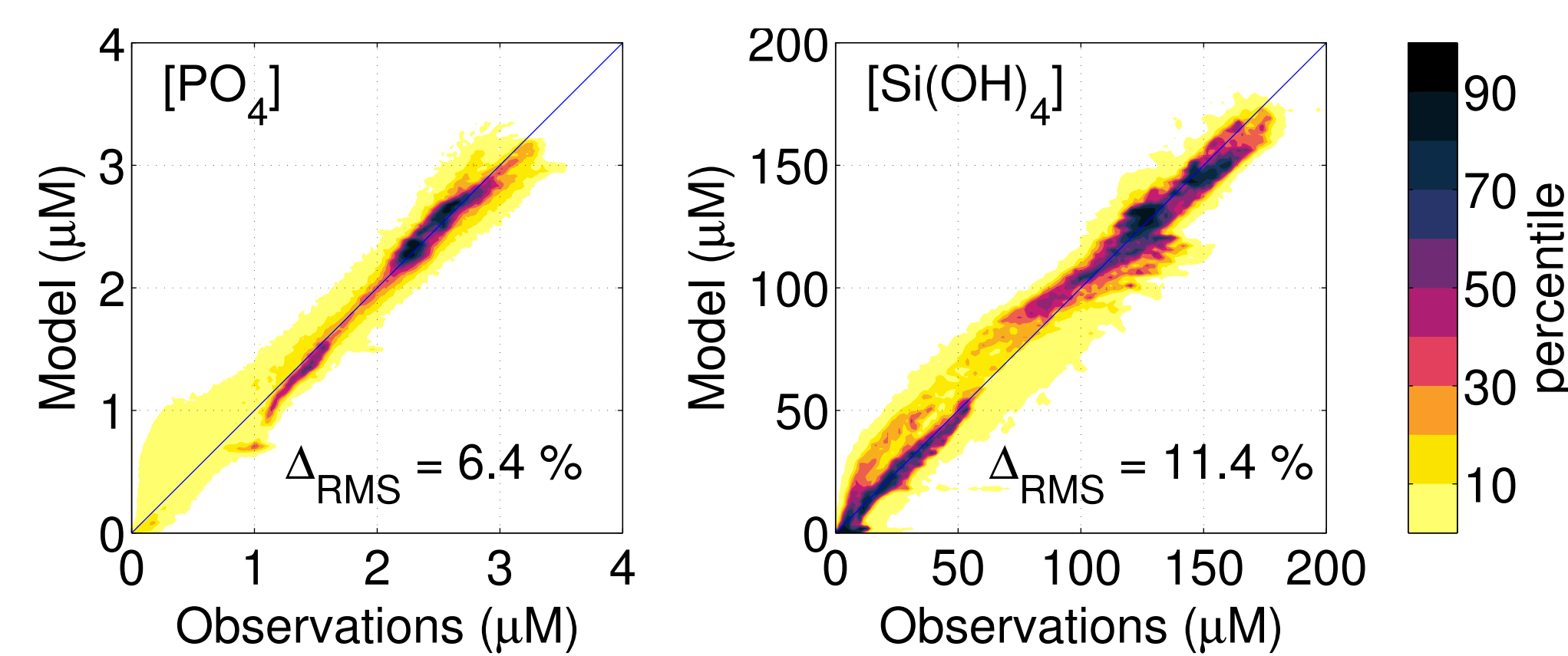

Figure 1. Joint distributions (binned scatter plots) of modeled and observed [PO_4] (left) and [$Si(OH)_4$] (right), expressed in percentiles.
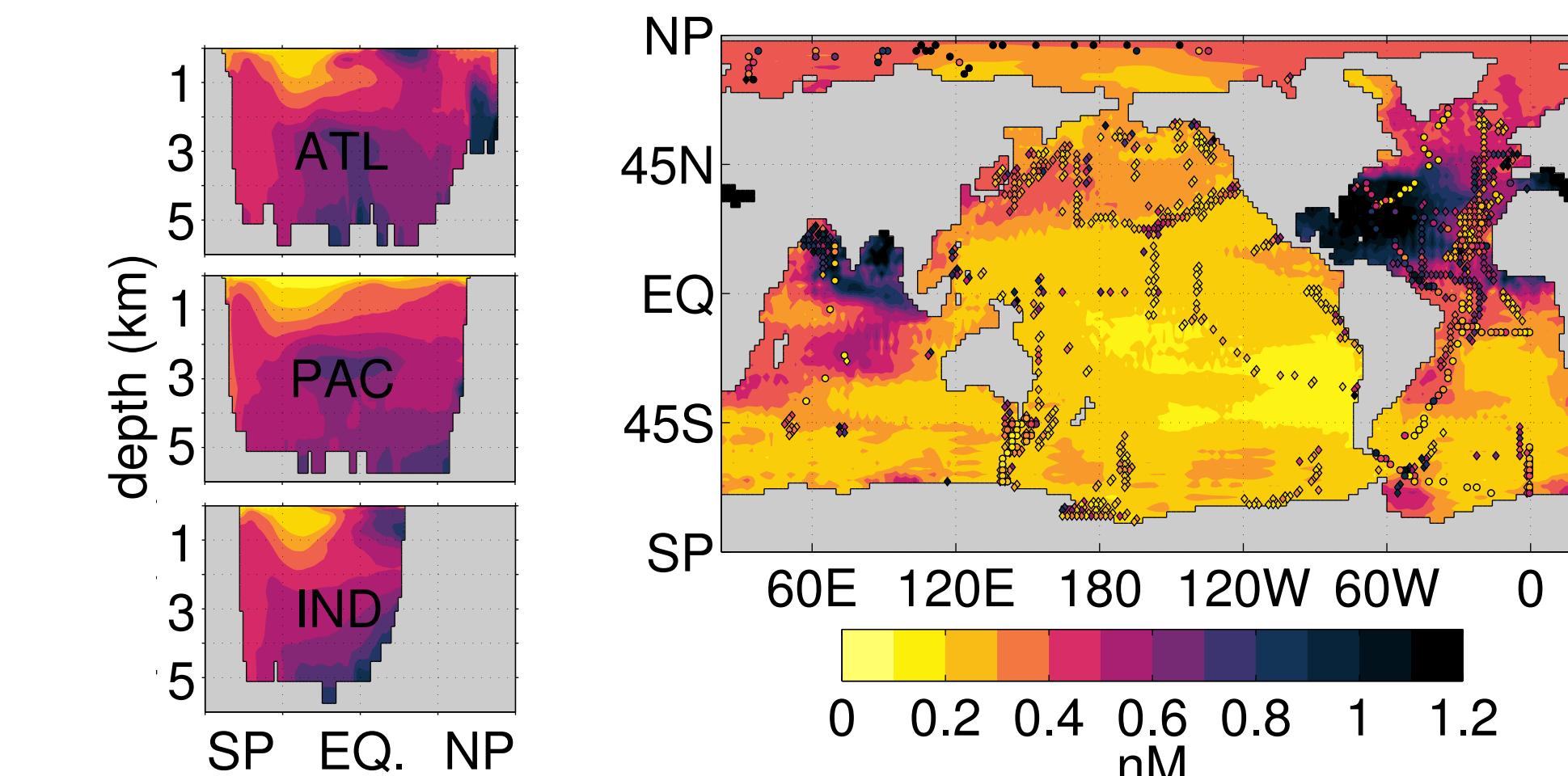
Dissolved iron concentration

Figure 2. Basin Zonal Averages (left) and euphotic mean concentration (right) of modeled dissolved iron. Circles and diamonds represent observations from the GEOTRACES [*Mawji et al.*, 2015] and the *Tagliabue et al.* [2012] data sets, respectively.
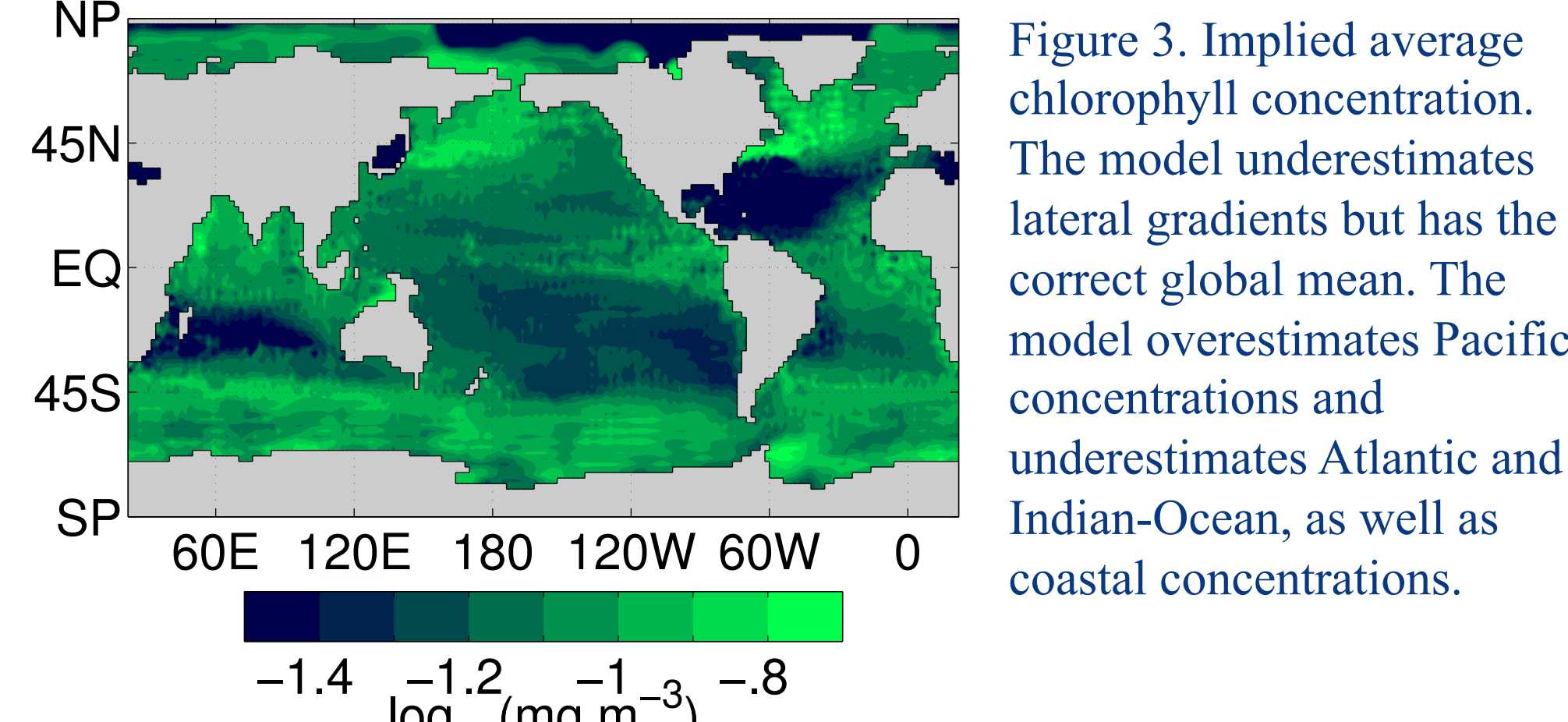
Implied surface chlorophyll concentration

Figure 3. Implied average chlorophyll concentration. The model underestimates lateral gradients but has the correct global mean. The model overestimates Pacific concentrations and underestimates Atlantic and Indian-Ocean, as well as coastal concentrations.

Nutrient deficiencies for Small, Large, and Diatom functional phytoplankton classes
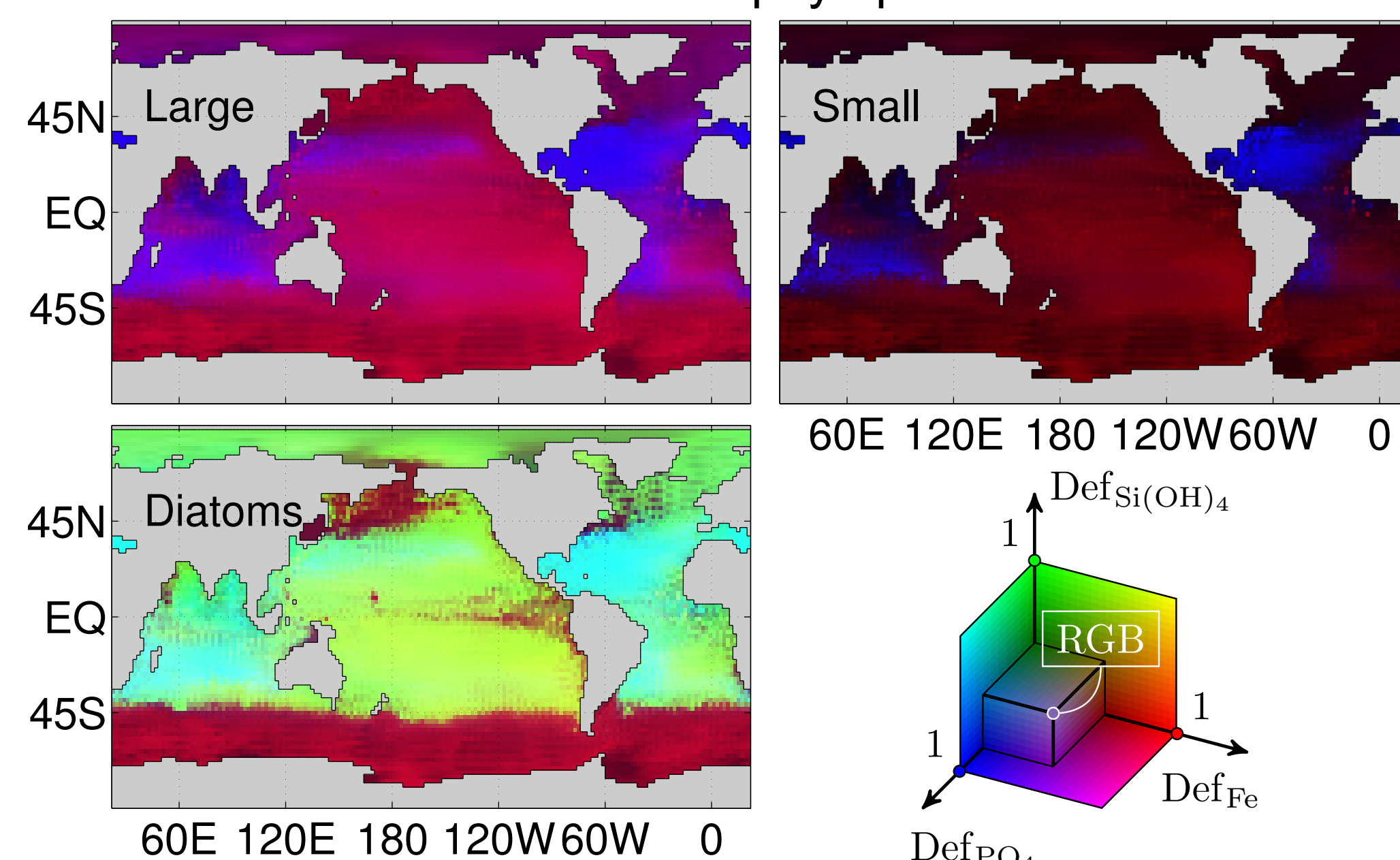

Figure 4. RGB representation of nutrient deficiencies Def$_X$, for each phytoplankton class and nutrient X. We define Def$_X$=1−m_X, where m_X's are the Michaelis-Menten factors of F_N. Red indicates iron limitation, blue indicates PO_4 limitation, and green indicates Si limitation (see legend).
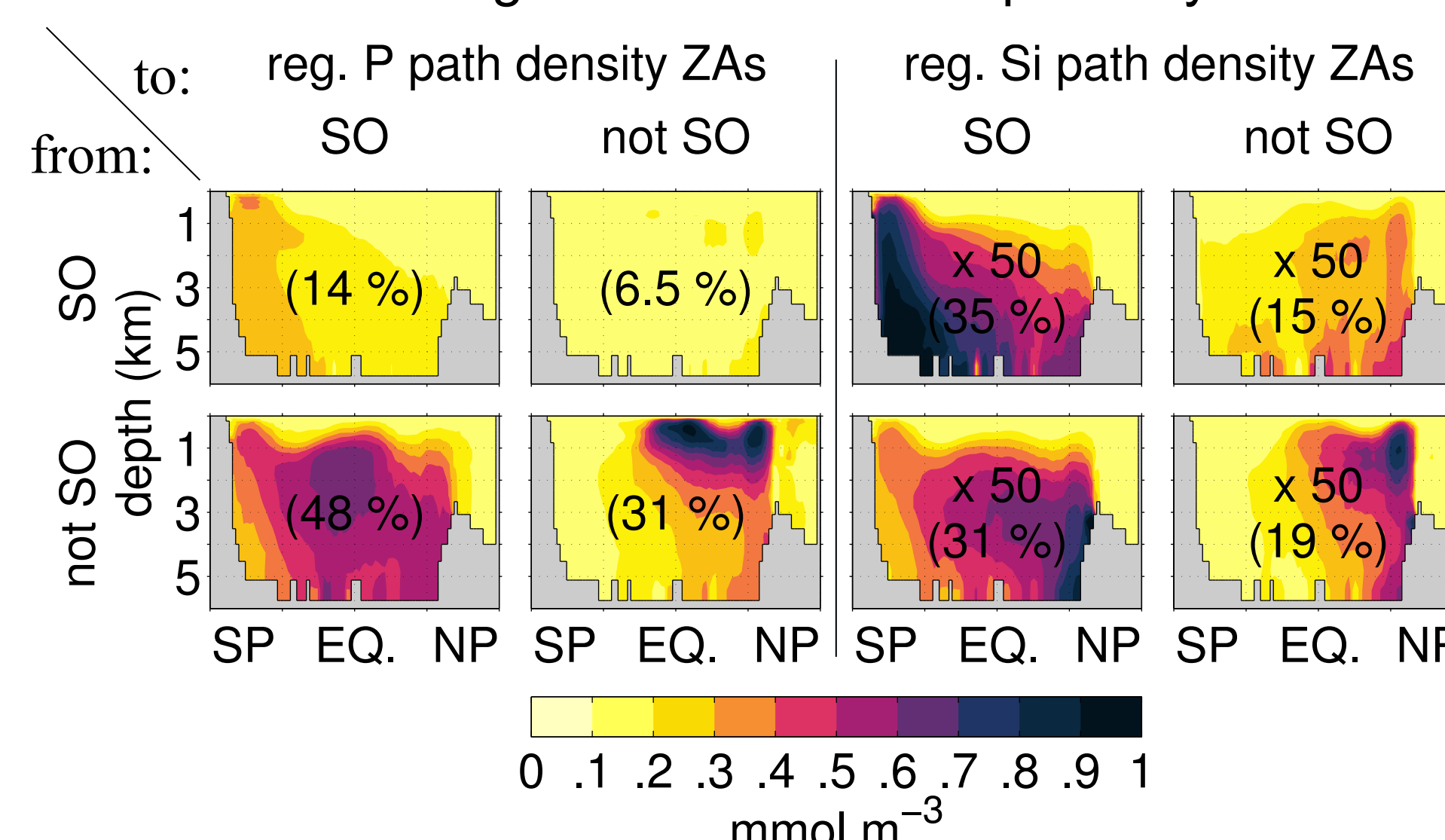
SO biological teleconnection pathways

Figure 5. Global Zonal Averages of the Path Densities of regenerated [PO_4] (left) and regenerated [$Si(OH)_4$] (right) exported from the SO (top) or outside of the SO (bottom) and reemerging in the SO (columns 1 and 3) or outside of the SO (columns 2 and 4). Ω_i→Ω_f path density at r is the local concentration that was last taken up and exported on Ω_i and that will reemerge on Ω_f: it quantifies the density of the nutrient molecules, and hence paths, at any interior point, that transit from Ω_i to Ω_f. Percentages of the global regenerated inventory are indicated in parenthesis (Note the scale multiplier for Si paths).

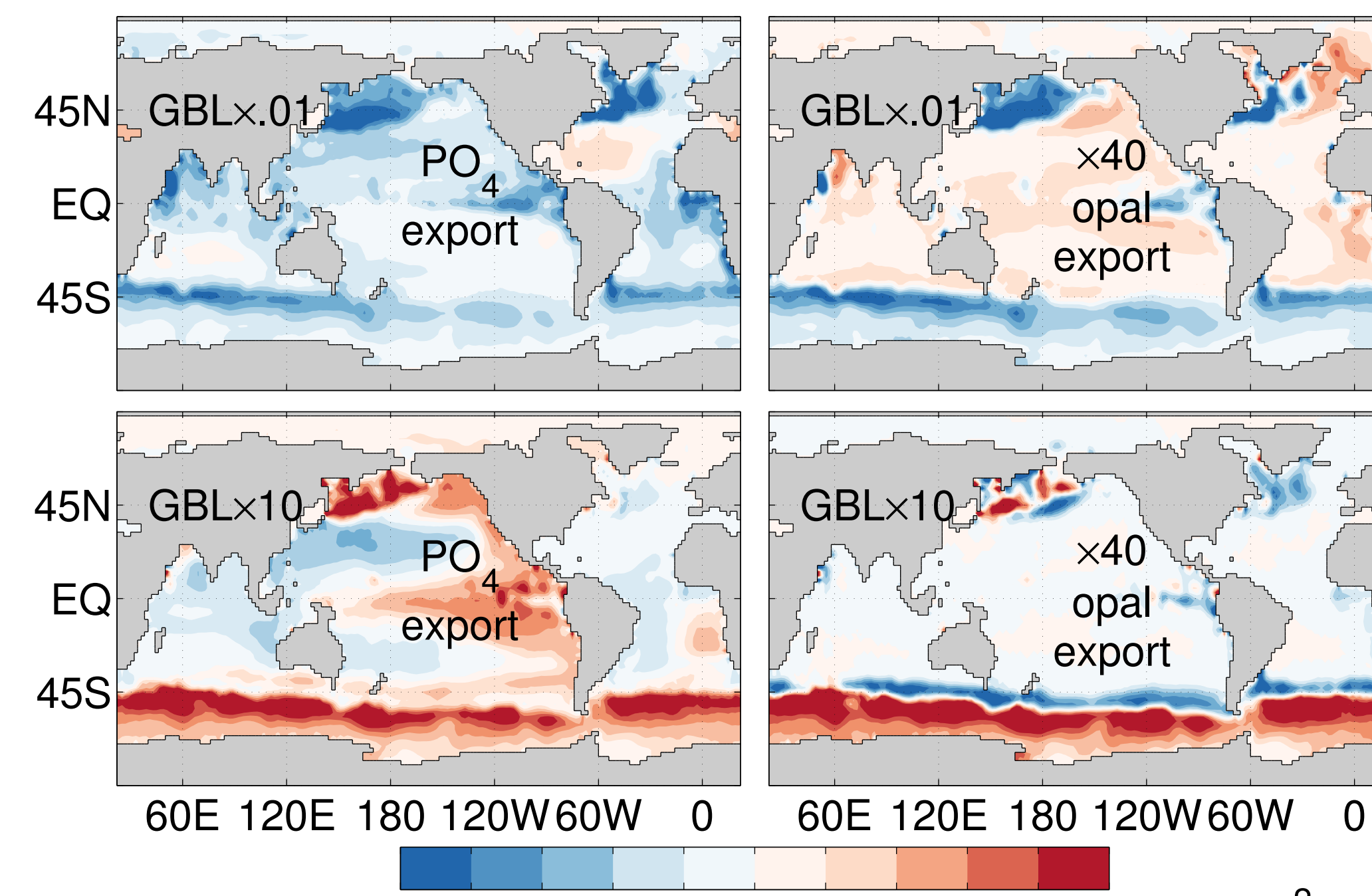## 4. Aeolian iron perturbations

Phosphorus and opal export responses

Figure 6. Response of the PO_4 export (left) and opal export (right; ×40) to a global uniform reduction (GBL×0.1, top) and increase (GBL×10, bot.) of the aeolian iron supply. Surprisingly, in the subtropical gyres, opal export increases for GBL×0.1, while PO_4 export decreases for GBL×10.

Response of the PO_4 and $Si(OH)_4$ pathways
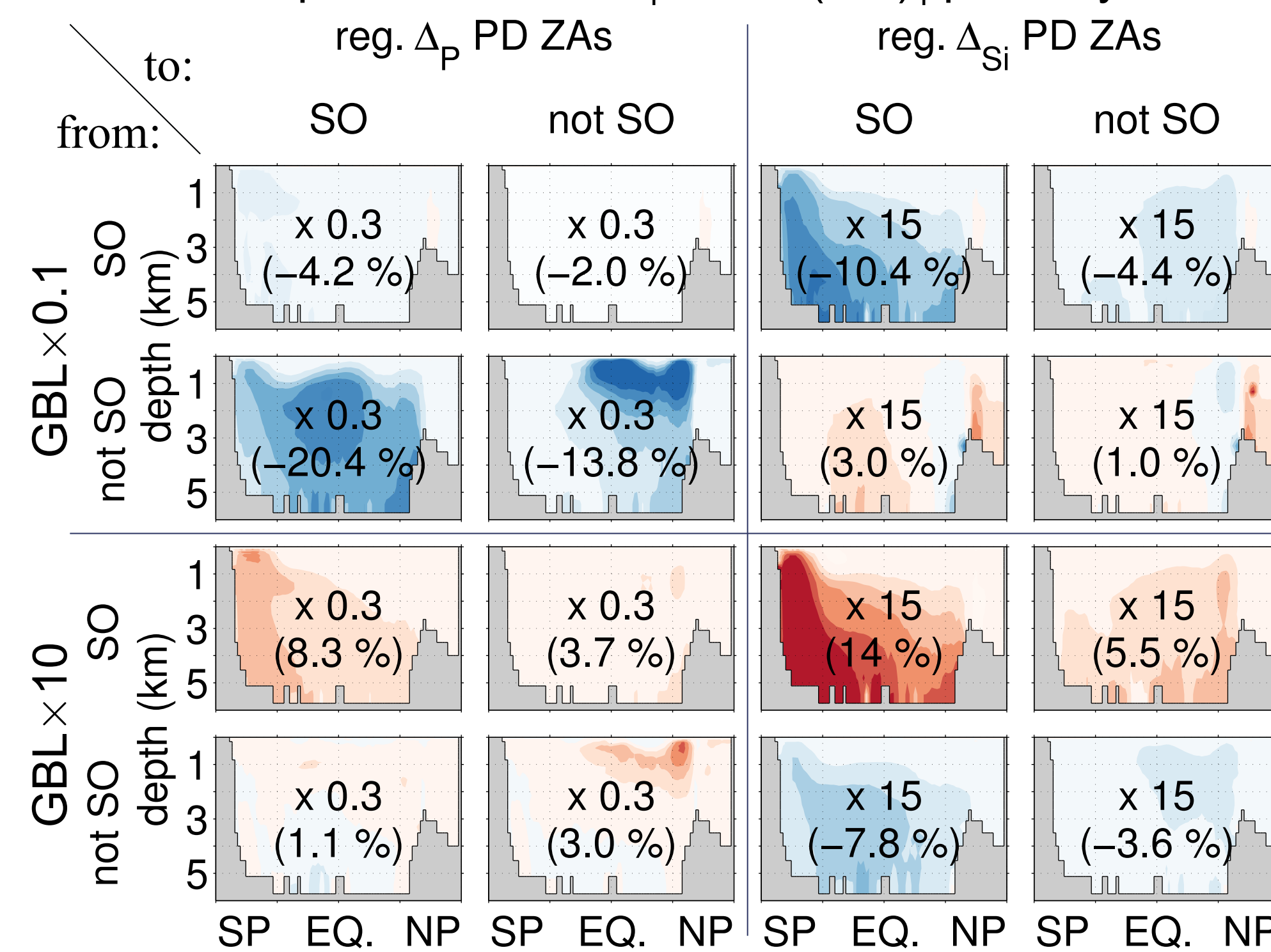

Figure 7. Response of regenerated Path Densities (Zonally Averaged, see Fig. 5) for GBL×0.1 (top) and GBL×10 (bottom) aeolian iron perturbations. Reduced iron decreases exported PO_4 globally, but increases opal export outside the SO. Elevated iron largely increases Si-trapping in the SO, and reduces opal export outside the SO.

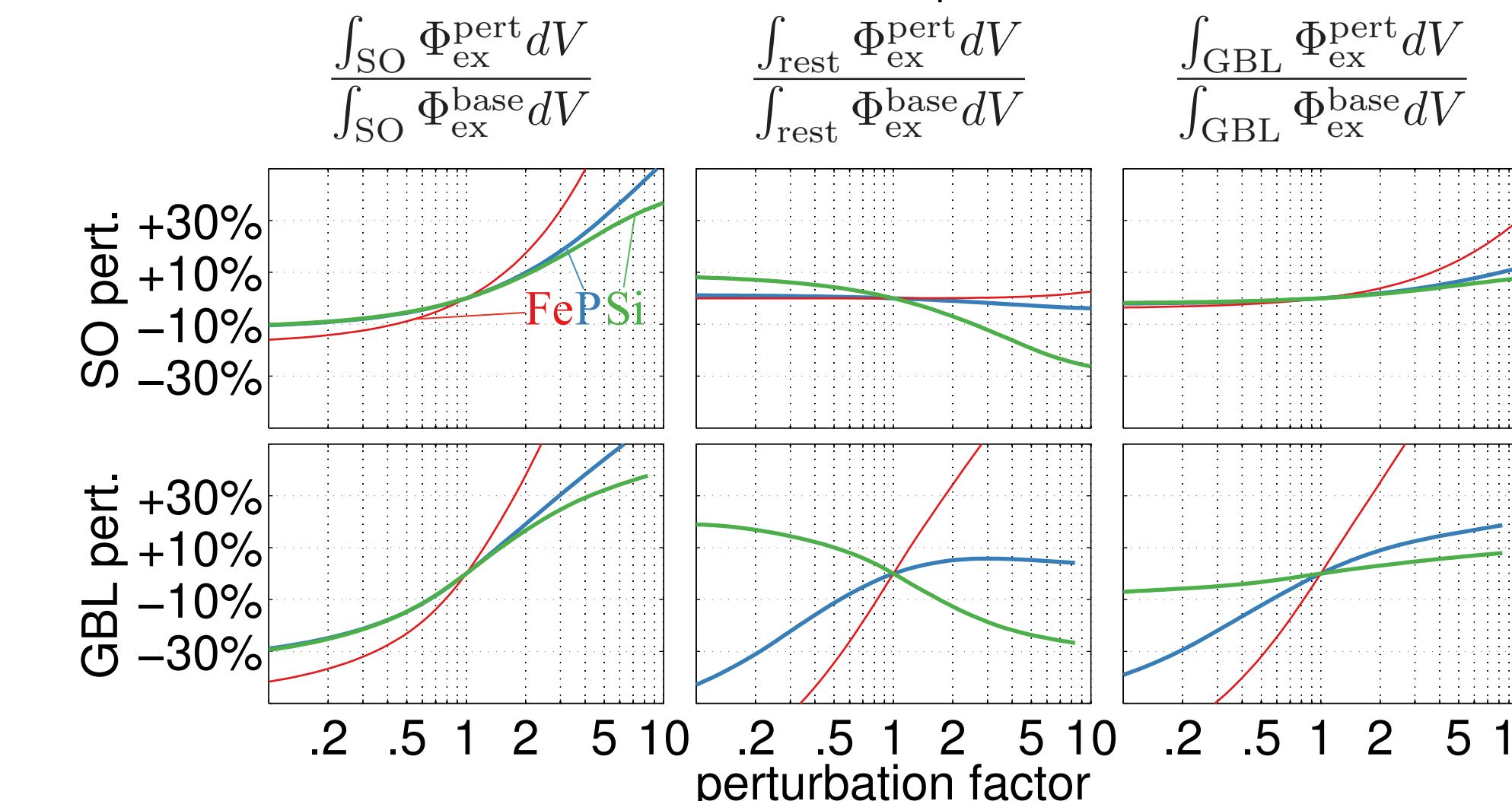### Response of basin integrated PO_4, opal, and iron exports

Figure 8. Response, relative to the base state, of PO_4 (blue), opal (green), and iron (red, thin) export productions, basin-integrated (SO: left | rest: center | GBL: right), for SO (top) and GBL (bottom) uniform aeolian iron perturbations. SO-integrated PO_4 and opal exports have asymmetric responses in strength for SO and GBL perturbations, and rest-integrated exports have asymmetric responses in sign for the GBL perturbation.

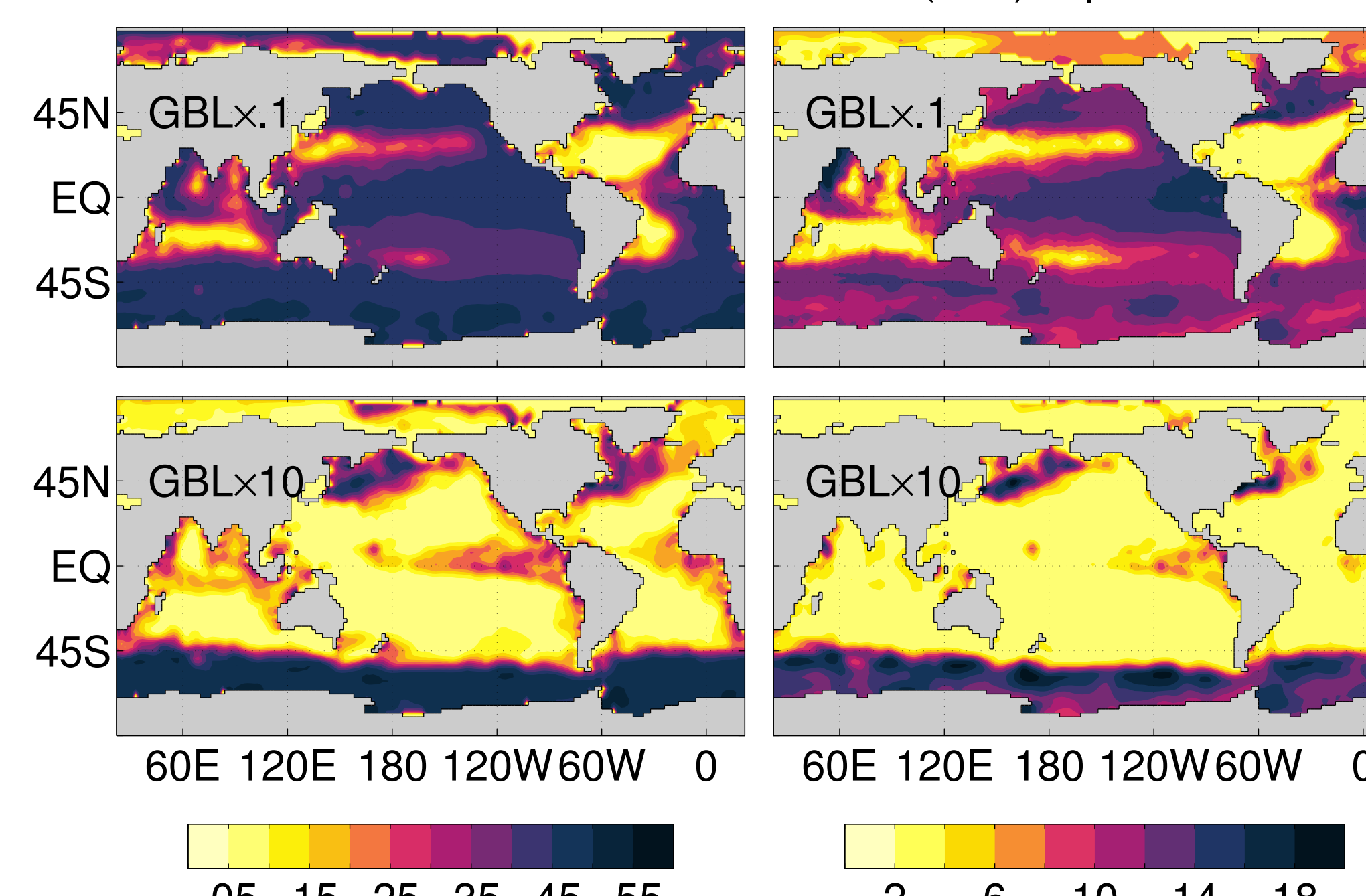### Response of Diatom fraction and (Si:P) export ratio

Figure 9. Perturbed biomass fraction of Diatoms f_D (left) and (Si:P) export ratio (right) for GBL×0.1 (top) and GBL×10 (bottom) aeolian iron input. Reduced aeolian iron input releases previously trapped Si from the SO, and thereby increases f_D and the (Si:P) export ratio in most of the ocean.

Response of the biological pump efficiency, the diatom fraction, and the (Si:P) export ratio
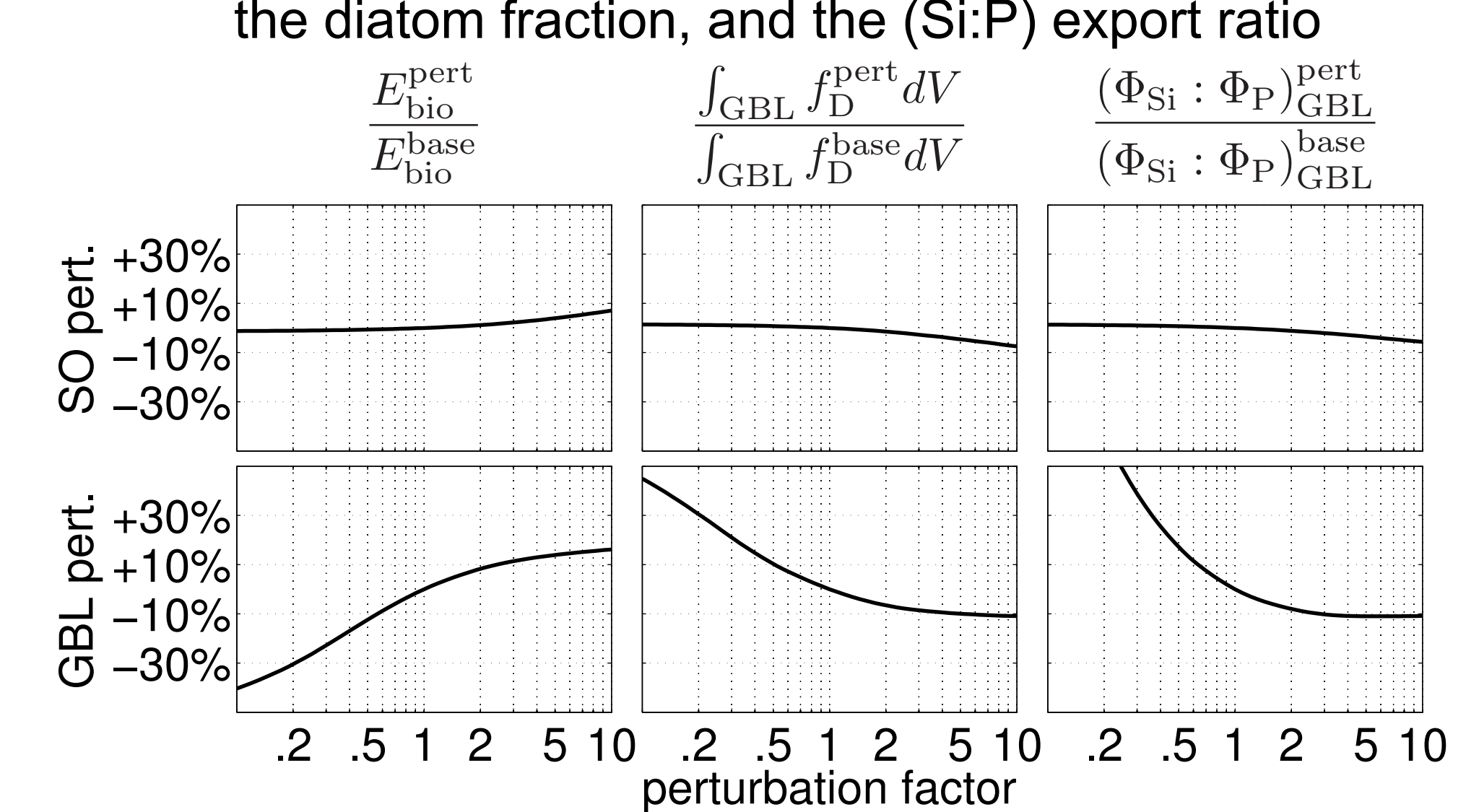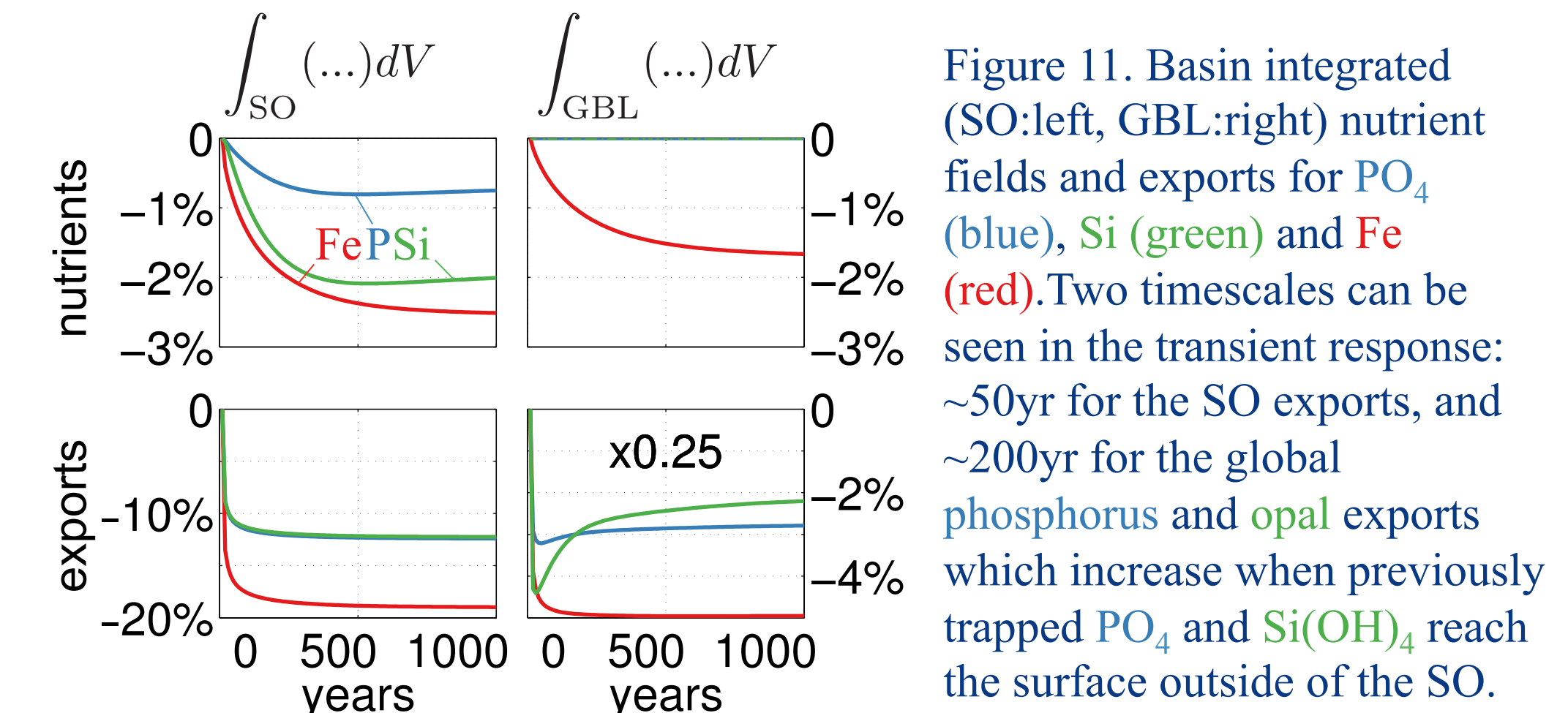

Figure 10. Response (relative to base state) of the global phosphate biological pump efficiency E_{bio}, (left), of the globally integrated Diatom biomass fraction f_D (center), and of the (Si:P) export ratio (right) for SO (top) and GBL (bottom) aeolian iron perturbations. SO perturbations have little effect, but responses to global perturbations are large, and reveal asymmetries in strength and sign.

5. Aeolian iron perturbations: Transient response

Transient response to sudden SO×0.1 perturbation

Figure 11. Basin integrated (SO:left, GBL:right) nutrient fields and exports for PO_4 (blue), Si (green) and Fe (red).Two timescales can be seen in the transient response: ~50yr for the SO exports, and ~200yr for the global phosphorus and opal exports which increase when previously trapped PO_4 and $Si(OH)_4$ reach the surface outside of the SO.

6. Conclusions

We constrained the biogeochemical parameters of the coupled {Fe, P, Si} cycle using a numerically highly efficient inverse model to minimize the mismatch with observed concentrations and chlorophyll. The model is then used to explore the effects of iron perturbations on the global nutrient cycling of phosphorus and silicon:

➤ The FePSi model captures the observed macronutrient concentrations (Δ_{RMS}(PO_4) ≃ 6% and Δ_{RMS}(Si(OH)$_4$) ≃ 11%) and produces a qualitatively realistic dFe field. The implied chlorophyll concentration matches satellite data in the mean, but still underpredicts lateral chlorophyll gradients (Figs. 1-3).

➤ The Small phytoplankton class has spatially well separated limiting regions, due to lower half-saturation rates compared to the Large and Diatom phytoplankton classes. The Small and Large classes are mostly iron-limited especially in HNLC regions, and Diatoms are Si-limited in the subtropical gyres (Fig. 4).

➤ The response to aeolian iron perturbations differs for the iron, phosphate, and silicon cycles (Figs. 5-8):
  • Globally uniformly increased aeolian input (GBL×10) increases P and Si exports at high latitudes (e.g. SO P-export +50% and Si-export +35%). Outside the SO, P-export also increases (+4%), while Si-export decreases (-30%) due to increased SO-trapping of Si.
  • Conversely, globally uniformly decreased aeolian input (GBL×0.1) decreases P-export globally. It also decreases Si-export in the SO (-30%), which releases previously SO-trapped silicon, increasing Si-export outside the SO (+20%).
  • For GBL×0.1, there is a strong decrease (-14%) in the rest→rest (rest = not SO) thermocline regenerated phosphate (P_{reg}) path and an even stronger decrease (-20%) in the deep diffusive rest→SO P_{reg} path, while the same Si$_{reg}$ paths are moderately increased (+1% and +3%).
  • Conversely, for GBL×10, there is only a weak increase in the same P_{reg} paths (+3% and +1%), but a stronger decrease in the Si$_{reg}$ paths (-4% and -8%).

➤ The (Si:P) export ratio and the global biomass fraction of Diatoms f_D are reduced (-5% and -8%) for SO uniformly increased aeolian input (SO×10), and are hardly increased (+3% and +2%) for SO uniformly decreased aeolian input (SO×0.1), due to the SO iron deficiency. Because of the asymmetry in strength and sign of the P and Si export responses, the (Si:P) export ratio and f_D are largely increased (+105% and +43%) for GBL×0.1 and decreased (-11% and -11%) for GBL×10 (Figs. 8-10).

➤ Again, because the SO is iron deficient, SO×0.1 has little effect on the global biological pump efficiency (-1%), while SO×10 increases it (+8%). However, it responds strongly to global perturbations (+17% for GBL×10 and -40% for GBL×0.1) (Fig. 10).

➤ Two timescales can be distinguished in the transient response for an abrupt aeolian input reduction: ~50yr for the SO export, and ~200yr for SO-released P and Si to increase export outside the SO (Fig. 11).

References

Frants, M., M. Holzer, T. DeVries, and R. Matear, **Constraints on the global marine iron cycle from a simple inverse model**, *J. Geophys. Research*, doi:10.1002/2015JG003111, 2016.

Primeau, F., M. Holzer, and T. DeVries, **Southern Ocean nutrient trapping and the efficiency of the biological pump**, *J. Geophys. Research*, 118, 2547-2564, doi:10.1002/jgrc.20181, 2013.

Galbraith, E. D., A. Guanabesikan, J. P. Dunne, and M. R. Hiscock, **Regional impacts of iron light colimitation in a global biogeochemical model**, *Biogeosciences*, 7, 1043–1064, 2010.

Matsumoto, K., K. Tokos, A. Huston, and H. Joy-Warren, **MESMO 2: a mechanistic marine silica cycle and coupling to a simple terrestrial scheme**, Geosci. Model Dev., 6, 477–494, doi:10.5194/gmd-6-477-2013, 2013.